Effect of Boundary Conditions on the Structure and Dynamics of Nanoscale Confined Water†

Jacob Goldsmith and Craig C. Martens*

Department of Chemistry, University of California, Irvine, Irvine, California 92697-2025

Received: October 1, 2008

In this paper, we investigate the effects of boundary structure on the properties of water in nanometer scale environments. We use molecular dynamic simulations to study water enclosed in model nanocavities with rigid boundaries of ice I_h structure and compare its behavior to that of water in cavities with smooth structureless boundaries. We show the dependence of quantities such as velocity autocorrelation function and hydrogen-bond lifetimes on the size and surface characteristics of the cavity. The boundary structure greatly influences the structure and dynamics of the water. In the smallest systems considered, with dimensions of 3−8 Å, the dynamics are slowed significantly, and the velocity autocorrelation function resembles that of solid ice.

Introduction

Water is an essential component of life, and its unique physical properties continue to inspire further investigation. A great deal of experimental and theoretical research has been directed at understanding the properties of water and aqueous solutions.[1−3] Despite this, much remains poorly understood and controversial. The anomalous properties of pure water, such as its high melting and boiling points and its density maximum at 4 °C, are well-known[2,4] but are still the subject of intense research. While some experimental work continues to focus on the structure and hydrogen-bond dynamics of bulk water via ^{1}H NMR[5] or X-ray diffraction,[6] other work has explored the modified properties of water in nanoscopic domains. Water in systems of nanoscale dimensions has been shown to have startlingly unique properties that can differ dramatically from bulk water. In the work of Korobov et al.,[7] differential scanning calorimeter measurements were used to determine the melting enthalpy of water prepared within nanodiamond gels. It was postulated that similar phases exist in other clusters of carbon nanoparticles whose size is smaller than 200 nm. Hydrated pores are another example of where water forms ordered structures in confined environments. Here, water forms cagelike wetting paths for flow within the pore.[8] Water filling a cavity is highly sensitive to the size of the cavity and the strength of the interaction between water and the cavity walls.[9] Wettability has been shown to be highly correlated to the physical nature of microstructures and nanostructures on a surface.[10]

A large number of recent computational studies have considered water and aqueous solutions in the confined environment of carbon nanotubes. These investigations highlight the effect that nanoscale size and structure can have on solutions. Mashl et al. investigated the properties of water under confinement in carbon nanotubes using molecular dynamics (MD) simulations.[11] For critical diameters, the water in the pore adopts a regular, icelike structure. Slight variations in the diameter leads to disordered, bulklike water, demonstrating the sensitivity of water properties to the geometry of boundaries on the nanoscale. Experiments have also probed water properties inside of carbon nanotubes.[12,13] For instance, Maniwa et al. have observed the formation of pentagonal to octagonal ice in carbon nanotubes.[13] In related studies, Levinger, Fayer, and coworkers have probed the dynamics of nanoscale water in reverse micelles using ultrafast infrared vibrational echo spectroscopy and observed significant differences in the rate of hydrogen-bond dynamics compared to bulk water.[14] Several groups have investigated the dynamics of water permeation through the membrane channel protein aquaporin.[15−18] Here, a narrow hydrophobic channel allows facile single-file transport of water molecules through the core of the protein. In related studies, a number of investigators have performed simulations and theoretical analysis of water dynamics in model nanopores.[11,19−36] These systems typically are chosen to be simple analogues of the hydrophobic channel in aquaporin. The small diameter systems studied exhibit rapid concerted transport of aligned water in a single-file fashion. Giovambattista et al. investigated hydration of confined water by nanoscale surfaces with patterned hydrophobicity and hydrophilicity.[37] Fluid flow in carbon nanotubes and nanopipes was recently reviewed by Whitby and Quirke.[38]

Aqueous solutions in nanopores and nanotubes have also received attention. Aluru and coworkers have performed molecular dynamics simulations of electrolyte solutions in carbon nanotubes to study ionic flow in models of protein channels in cell membranes[39] and interfacial effects in KCl transport in charged silicon nanochannels.[40] This group has also studied the single-file osmosis of water through a semipermeable membrane spanned by charged and uncharged nanopores.[41]

Salt solutions in nanopores have also been investigated theoretically by Hansen and coworkers.[42] In these studies, the ability of ions to enter water-filled pores can be affected by external electric fields, suggesting nanoscale control of solutes. Yang and Garde modeled the selective partitioning of cations into negatively-charged nanopores in water.[43] Hydrated pores are another examples of where water forms ordered structures in confined environments. Here, water forms cagelike wetting paths for the flow of water within the pore.[8] Water filling a cavity has been shown to be highly sensitive to the size of the cavity and the strength of the interaction between water and the cavity walls.[9]

The so-called core−shell model in reverse micelles has been proposed[44,45] to describe the water directly hydrating the anionic

† Part of the "Max Wolfsberg Festschrift".

* To whom correspondence should be addressed. E-mail: cmartens@uci.edu.

10.1021/jp808709v CCC: $40.75
Published on Web 02/17/2009

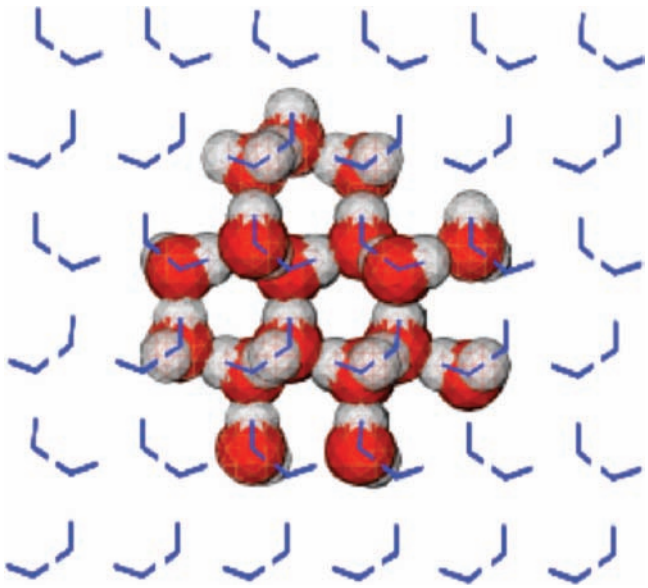

Figure 1. System structure for the r6 simulation. The water molecules shown as line drawings (blue) are held fixed in the (I_h ice) structure, while the waters drawn with their van der Waals radii (red and gray) are mobile.

surfactant aerosol and the water not in contact with the anion. The core−shell model aims to describe microensembles of hydrogen-bonding networks, which get disrupted at the surface of the micelle. Chanda et al.[46] used MD to calculate the lifetimes of hydrogen bonds as a function of the location of this formation. While both systems studied the hydrogen bonding near highly polar head groups, these studies failed to isolate the region in which only water−water interactions contributed to the dynamics.

In this paper, we investigate the effects of boundary structure on the properties of water in nanoscale environments. We employ the method of molecular dynamics (MD) simulations[47] to study water enclosed in cavities surrounded by rigid boundaries of ice I_h structure and compare its behavior to that of water in cavities with smooth structureless boundaries. We calculate dynamical quantities such as the velocity autocorrelation function and hydrogen-bond lifetime distributions and analyze their dependence on the size and surface characteristics of the cavities.

Systems and Methodology. We study an idealized model of water in nanoscale environments. In particular, we consider water in (roughly) spherical voids in a rigid material. Two cases are considered: hydrophilic voids with structured boundaries built on a rigid ice geometry and voids enclosed in smooth structureless walls. The structured boundaries are defined by a rigid solid with an ice I_h structure enclosing a sample of dynamically mobile water molecules within a radius r_{sphere} of the origin. The structureless voids are defined by applying a radial harmonic restoring force on atoms with $r > r_{sphere}$.

The hydrophilic voids are constructed by selecting water molecules in an initial ice I_h structure whose oxygen atoms are greater than a distance r_{sphere} from the origin. This outer section of the ice remains spatially fixed during the molecular dynamics simulations, while the waters within the void are allowed to move (see Figure 1). This system is physically unrealizable but offers a simple model for studying the effect hydrophilic confinement. In particular, the ice surface structure acts as an optimal "template" on the dynamically mobile waters within and thus might be expected to induce icelike structure and dynamics in the liquid phase.

TABLE 1: Summary of Rigid Ice Boundary Simulations and the Spherical Boundary Comparison Runs[a]

	rigid ice boundary		spherical boundary	
system name	waters	avgdensity	waters	avgdensity
r4	11	0.085	11	0.056
r6	33	0.036	33	0.037
r10	69	0.037	65	0.035
r15	389	0.032	469	0.031
$bulk_{NVT}$			3905	0.031
$bulk_{NVE}$			3905	0.031

[a] The density is given in waters per Å^3. Here, r4, r6, r10, and r15 are the simulation names and indicate the approximate radial size of the void. The approximate scale of each from r4 to r15 is 3, 6, 8, and 14 Å, respectively.

The calculations described here are carried out using the NAMD molecular dynamics package, developed by the Theoretical and Computational Biophysics group in the Beckman Institute for Advanced Science and Technology at the University of Illinois at Urbana−Champaign (UIUC).[48] Visualization and data analysis are conducted using VMD, a visualization package also available from UIUC.[49]

A summary of the system configurations studied is found in Table 1. The systems are denoted r4, r6, r10, and r15, indicating the approximate radii of the void. For each void size considered, two systems are treated: a hydrophilic structured boundary model as described above and a system of (roughly) the same size with a smooth and structureless spherical boundary for comparison. In addition, bulk water simulations are performed, and the results are compared with those of our confined models. These systems consist of a similar number of waters and density confined with a spherical boundary condition (SBC) algorithm (see Table 1). The SBC algorithm for a harmonic restoring potential directed toward the origin has the form:

$$E_{sbc} = \begin{cases} k_{sbc}(|\vec{r}_i| - r_{sphere})^2 & |\vec{r}_i| > r_{sphere} \\ 0 & |\vec{r}_i| < r_{sphere} \end{cases} \quad (1)$$

where k_{sbc} is the force constant, $\vec{r}_i$ is the position of the i^{th} molecule (relative to the origin at the center of the cavity), and r_{sphere} is the radius of the spherical cavity. External forces of this form are implemented in NAMD.[48] Our SBC simulations employ an r_{sphere} and k_{sbc} chosen to give a density as close to the bulk value as possible (0.032 waters per Å^3). Our bulk simulations consist of ca. 4000 water molecules and are thus much larger than our confined water simulations. SBC simulations gave densities reasonably close to bulk water, as shown in Table 1.

All systems are initially thermalized at a temperature $T =$ 300 K using a Langevin thermostat in order to create a starting point for constant energy (NVE) simulations, which are used to collect data. Output for velocity and positions are recorded every 1 and 5 fs for velocity autocorrelation functions and hydrogen-bond dynamics, respectively. Observables were averaged over a number of simulations as described below. Because of the small number of free waters and icelike dynamics, longer simulation times (e.g., 0.5 ns) are needed for r4 and r6 simulations so that sufficiently large data sets are generated for statistical analysis.

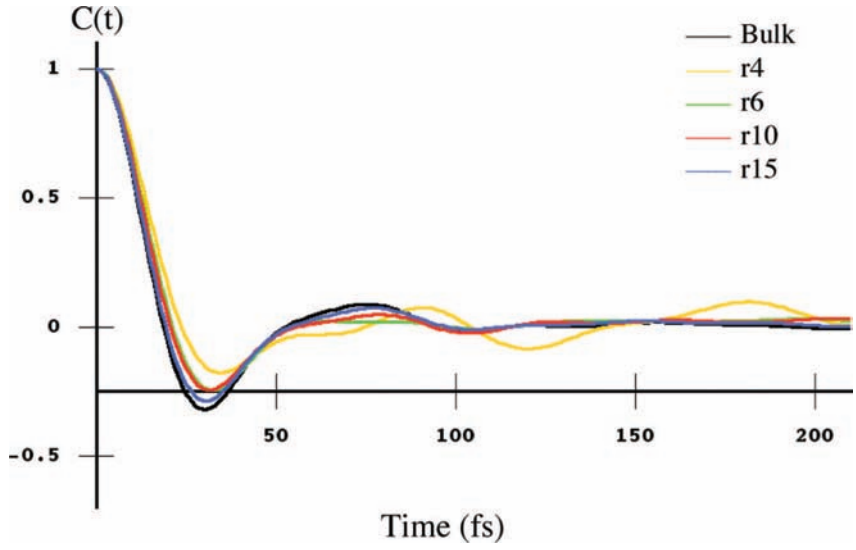

Figure 2. The velocity autocorrelation function (VACF) for spherical boundary water simulations, compared with the bulk result. See text for discussion.

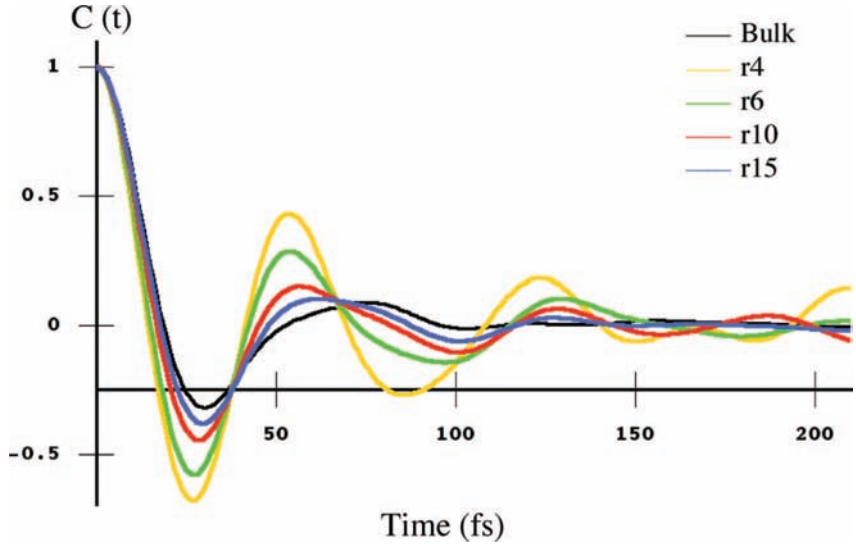

Figure 3. The velocity autocorrelation function (VACF) for our templated boundary water simulations, compared with the bulk. See text for discussion.

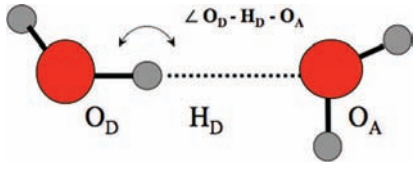

Figure 4. The geometric criterion used with the defining hydrogen bonds in terms of intermolecular lengths and angles: $\theta = 150°$ and length $O_{donor}-O_{acceptor} = 3.5$ Å.

Results

We calculate the velocity autocorrelation function (VACF) $C(t)$ for each simulation. The VACF is found by computing the following averages over the ensemble:[47]

$$C(t) = \frac{\langle v(0) \cdot v(t) \rangle}{\langle v(0) \cdot v(0) \rangle} \quad (2)$$

Here, $v(0)$ and $v(t)$ are the velocities at time $t = 0$ and a later reference time t, respectively, while the <... > is an average over both the molecules in the system and time. The results for this calculation are shown in Figure 2 for SBC simulation and Figure 3 for confined simulations. The results are averages over three independent MD simulations.

TABLE 2: Average Hydrogen-Bond Lifetime and Average Number of Hydrogen Bonds per Water[a]

	confined simulation		spherical boundary	
simulation	τ_{HB}	HB per water	τ_{HB}	HB per water
r4	2984	1.2	169	1.1
r6	1759	1.2	200	1.3
r10	315	1.3	194	1.4
r15	236	1.5	202	1.6
$bulk_{NVT}$			194	1.7
$bulk_{NVE}$			214	1.7

[a] The average lifetime and the average number of hydrogen bonds do not include interactions with the wall. The lifetimes and average hydrogen bonds per water are averaged over three independent simulations. Lifetimes (τ_{HB}) are given in units of femtoseconds. The table reports averages using the $O_{donor}-O_{acceptor}$ distance and the $O_{donor}-H_{donor}-O_{acceptor}$ angle criterion described in the text.

Hydrogen bonding is a dominant contribution to the structure and dynamics of water. There has been a great deal of discussion

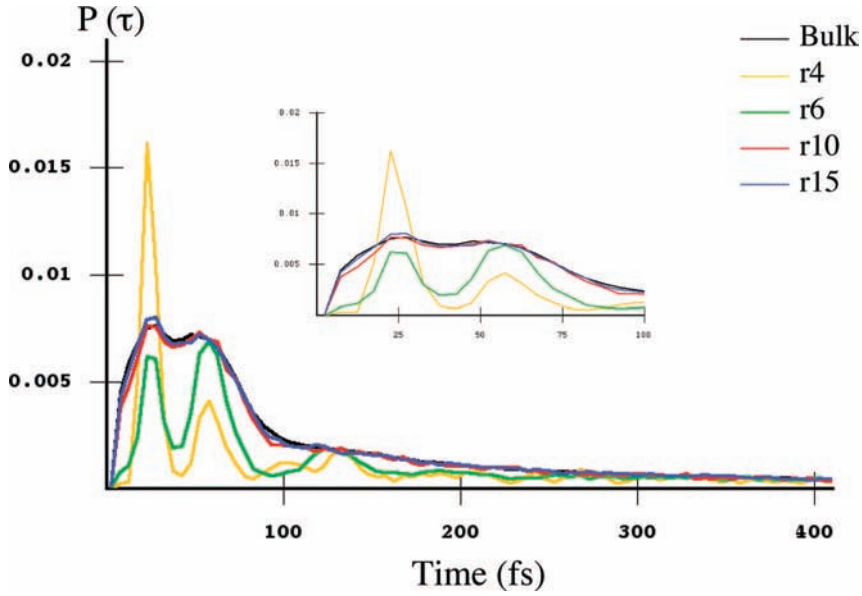

Figure 5. The normalized probability density function (PDF) for the smooth boundary confined systems, as described in the text. The spherical droplets have similar PDFs as the bulk simulation.

in the literature regarding the advantages of various hydrogen-bond definitions that are employed in analyzing the data generated by MD simulations of water and aqueous solutions. In terms of the dynamical variables, the two main approaches are the geometric method,[50] based on the pair correlation function $g(r)$ extracted from NMR or neutron X-ray diffraction, and the energetic method,[51] which is related to activation energies measured by IR and Raman spectroscopy OH and OD shifts. Both methods have various alternative definitions and hybrid forms.[52] An ideal model for hydrogen bonding should be one which can be compared to NMR (for angles)[5] and XRD (distances between bonds)[6] experiments. That is, a model should be comparable to bulk water and converge to values close to bulk water values. It is believed that geometric criterion fit to NMR experiments are better than energetic criterion,[53] but most methods produce comparable results.

Of the available methods, we choose to use the geometric criterion to define hydrogen bonds, which is defined by three conditions on the atomic coordinates: (1) the $O_{donor}-O_{acceptor}$ distance should be less than 3.5 Å; (2) the $H_{donor}-O_{acceptor}$ distance should be less than 2.5 Å; (3) the bond angle θ created by the $O_{donor}-H_{donor}$ vector and the $H_{donor}-O_{acceptor}$ should be less than 150°.[54] A summary is shown in Figure 4. In this work, we use the angle cutoff and the $O_{donor}-O_{acceptor}$ distance. Average hydrogen bonds per water are within the accepted values for a bulk water simulation using our criterion.[55] A summary of the hydrogen bond analysis is shown in Table 2.

The method used converges well with the strict geometric criterion and the energetic criterion in NVT bulk simulations.[51] It should be noted that this criterion can also have a very close analogy to the energetic method simply by relaxing some of the conditions (and applying some trigonometry). For example, when we relaxed our angle criterion and used the $H_{donor}-O_{acceptor}$ distance, similar values were obtained as compared to an energetic criterion.[51] Note that the difference in the lifetimes is due mostly to the environment surrounding the water molecules, while the number of hydrogen bonds fluctuates because of the surface area of the outer edge of a simulation (i.e., the outer surface excludes the formation of hydrogen bonds explicitly in the SBC boundary, while in the confined simulation the outer surface implicitly excludes the counting of hydrogen bonds to the walls).

In the work of Luzar,[56] the hydrogen-bond correlation function is described and later extended by Chanda et al. into two distinct time correlation functions,[46] the continuous correlation function and the intermittent correlation function. Generally, these are fit to multiexponential functions thus defining the hydrogen-bond lifetimes. This method has also allowed treatment of hydrogen bonds as an activated process and uses the lifetime within the Eyring equation to calculate activation energies.[53] In our work, we simply use a time average of the intermittent lifetimes so that the hydrogen bonds are treated as broken when any test of the hydrogen-bond criterion is false. Numerically, this is expressed as

$$\tau_{HB} = \frac{1}{N}\sum_{i}^{N} h_i \tag{3}$$

where h_i is the i^{th} hydrogen-bond lifetime and the sum is over N hydrogen bonds that broke during the total sample time. To record the lifetime, each lifetime is initialized to 0 and are recorded only after any initial bonds break. We sample the criterion in 5 fs increments, as was shown in the literature to be adequate to capture the fast dynamics of the hydrogen bond.[53]

Hydrogen-bond networks are generally thought of in terms of thermal fluctuations over the inherent structure of water.[57] The dynamics are then divided into a fast component and slow, diffusive component. The two components of hydrogen bond dynamics are often examined via the hydrogen-bond correlation function's slow and fast decay constants. Instead of calculating the correlation function, we calculate the probability density function (PDF) for the hydrogen bond lifetimes:

$$\mathrm{PDF}_{HB}(\tau) = \frac{P(\tau)}{\int_0^{\infty} P(\tau)\, d\tau} \tag{4}$$

Here, the numerator $P(\tau)$ represents the histogram of lifetimes (recorded at the time of breaking), and the denominator is the normalization factor (where, in practice, "∞" is over a sufficiently long simulation time). A plot of the PDF's for the confined and SBC are shown in Figures 5 and 6, respectively. Similar to the behavior of the correlation function, a sharp fast decaying peak and a slow decaying tail are seen in the Figures, while the confined simulations show further structure in the PDF.

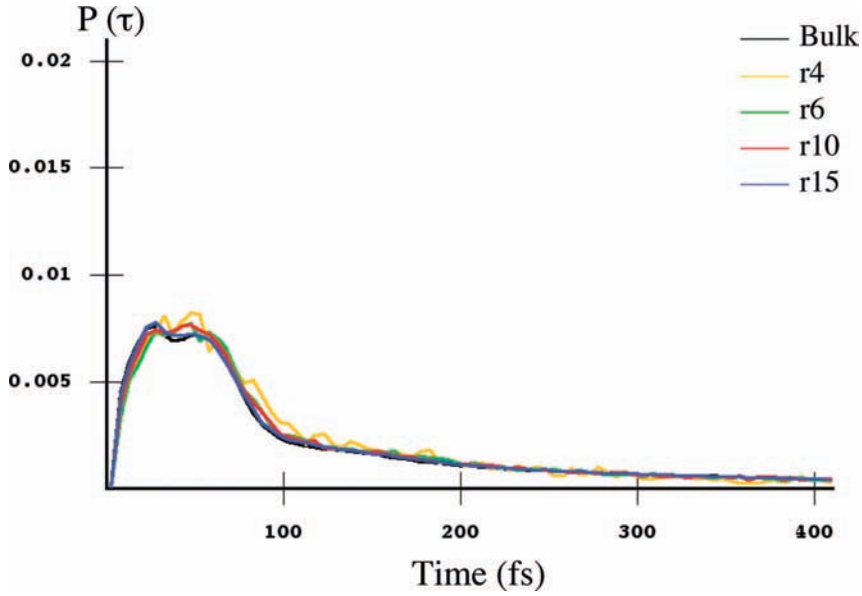

Figure 6. The normalized probability density function (PDF) for the templated boundary confined systems, as described in the text. The PDFs for short distances for the confined r4, r6, and the bulk system is show in the insert to more clearly display the structure of the confined systems.

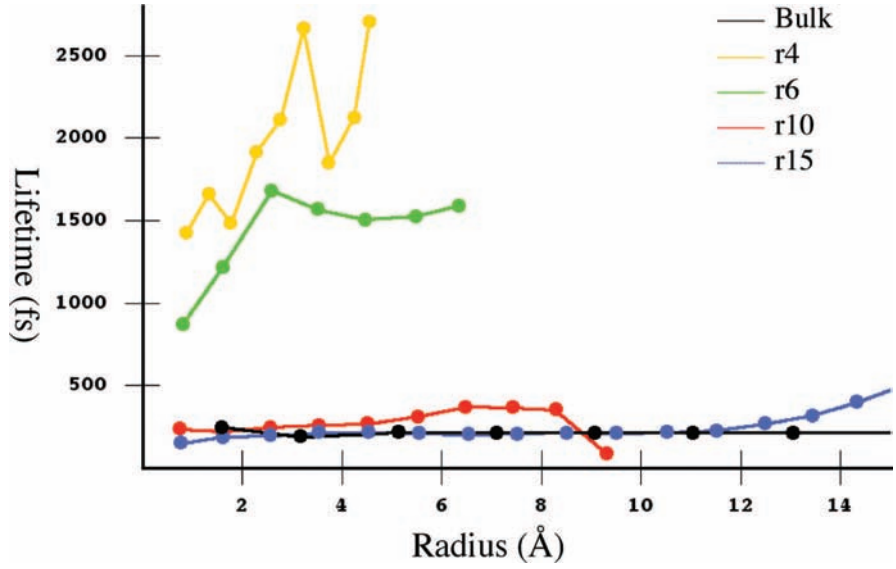

Figure 7. Histograms of hydrogen-bond lifetimes as a function of radial position. The bin sizes are 0.5, 1, 1, 1, and 2 for r4, r6, r10, r15, and bulk, respectively. See the text for discussion.

In order to understand radial layering and structuring effects in the confined water, we examine the spatial dependence of the hydrogen-bond lifetimes. Here, we used the breaking point of the hydrogen-bonded acceptor hydrogen spatial positions to calculate $\vec{r}_i$. Since the ratio of the size of a water molecule to the system size is large compared to bulk, significant dynamical affects are expected at the boundaries of the system. The results of a histogram of average $\vec{r}_i$ versus lifetimes is shown in Figure 7 and discussed below.

The diffusion constant for our bulk water simulation is calculated from the integral of the VACF with respect to time. The value obtained from the integral is close to bulk values reported previously.[58] From Figures 2 and 3, the confined simulations have a tendency to have larger oscillation and a slower decay to zero. This is seen in the VACFs as a slower decay of $C(t)$ as compared to bulk VACF. In particular, the r4 and r6 templated boundary simulations show dynamical oscillations from limited degrees of freedom. This is a clear indication that the surrounding potential alters the dynamics on the scale of 3−8 Å. The behavior of the confined simulations converge toward that of the bulk as the cavity size gets larger. The smooth boundary droplets, on the other hand, show little variation with size and exhibit bulklike VACFs for all cases studied.

Discussion and Conclusions

From the average lifetimes given in Table 2, one can see that the smooth boundary confined systems have values close to bulk for all the simulations, while the templated boundary confined systems exhibit longer hydrogen-bond lifetimes. The smaller simulations exhibit larger probabilities near the peaks suggestive of solid phonons in the VACF, and tails, which decay over longer time periods. In general, the average number of hydrogen bonds per water shown in Table 2 increases with size of the system and increases from a SBC simulation compared to a templated boundary simulation. Generally, the larger the surface area to volume ratio, the longer lived the hydrogen bonds.

It is also noteworthy to compare the PDFs of the smooth and templated systems. The most probable hydrogen-bond lifetime is very similar from simulation to simulation, as can be seen from Figure 6. The PDF has two peaks at about 30 and 60 fs, which are at the first and second zeros in the VACF (the forward and reverse relative velocity correlations). The smaller systems show sharp peaks at those values, while the larger simulations are smoother. Finer bin sizes or larger output frequencies do not resolve these peaks. The tail of this function is related to the diffusion for longer times. As the system are made smaller, the number of hydrogen bonds available is decreased, and the inherent tetrahedral structure of water is more prevalent. This leads to less mobility due to stronger hydrogen bond correlations. Such correlation is shown in various confined simulations, such as reverse micelles or single-file water in (6,6) carbon nanotubes.[19,44]

Histograms of the spatial dependence of the hydrogen-bond lifetimes show confinement or local templated environmental ordering, and one can infer that the dynamics are significantly slower near the structured hydrophilic boundary. In Figure 7, the lifetime is shown to increase near the wall of the smaller templated systems. The spherical boundary systems, on the other hand, look approximately like the bulk, a flat line near the average value of the lifetime. Slight downturns at the boundary can be attributed to the exact nature of the wall structure for a given size (i.e., radial values at the boundary that are predominantly oxygen atoms). The behavior found in these model systems is similar to that found spectroscopically in confined systems with structured boundaries[45] and might give insight into the effects of interfacial nanoconfinement in reverse micelles or similar structures.

It is evident from the simulations that the lifetimes of hydrogen bonds in a network is enhanced by templating interactions with the structured wall. By comparing the r6 and r10 trials, one can see a distinct lengthening of the lifetimes. In work by Jinesh and Frenken, room-temperature ice is observed in between graphite and a tungsten tip during friction force microscope[59] over distances on the order of 4 Å. This confinement is similar to r4 confined simulation in that VACF and narrow peaks in hydrogen-bond life times are observed similar to icelike structure and fit the characteristic lattice period of hexagonal ice. It seems reasonable that other structures can induce icelike water between 3 and 6 Å if confined between surfaces.

In the paper, we have explored the modification of the properties of water when confined in nanoscale volumes. We observe that local environment indeed affects the structure and dynamics of water. The magnitude of the effects of confinement greatly depend on the number of hydrogen bonds available per water as well as lifetime of nearby hydrogen bonds. Water shows a smoothing of the "local tetahedral" structure as it goes from confined template environment to bulklike environments. The extent of nanoconfinedment shown in this model situation is between 3 and 8 Å. For smaller systems, local order is prevalently dominant, while the larger systems tend toward bulklike dynamics near the center of the cavity. The effects depend strongly on the structure of the boundary, with nanosystems with smooth boundaries exhibiting behavior similar to the bulk down to very small sizes. Further work on this subject will be directed toward understanding the detailed dependence of water structure and dynamics on the characteristics of the molecular structure of the boundary. Other work attempts to take advantage of the special properties of water in nanoscale environments to study nanofluidic rectifiers.[60]

Acknowledgment. The authors would like to thank Doug Tobias, Ryan Benz, and Neelanjana Sengupta for helpful discussions. We thank the Network and Academic Computing Services (NACS) at UC Irvine for providing computer resources for some of these simulations.

References and Notes

(1) Tait, M. J.; Franks, F. *Nature* **1971**, *230*, 91.
(2) *Water: A Comprehensive Treatise*; Franks, F., Ed.; Plenum: New York, 1981.
(3) Ball, P. *Life's Matrix: A Biography of Water*; Farrar, Straus, & Giroux: New York, 1999.
(4) Berry, R. S.; Rice, S. A.; Ross, J. *Physical Chemistry*, 2nd ed.; Oxford University Press: Oxford, U.K., 2000.
(5) Modig, K.; Pfrommer, B.; Halle, B. *Phys. Rev. Lett.* **2003**, *90*, 075502.
(6) Wernet, P.; Nordlund, D.; Bergmann, U.; Cavalleri, M.; Odelius, M.; Ogasawara, H.; Näslund, L.; Hirsch, T.; Ojamäe, L.; Glatzel, P.; Pettersson, L.; Nilsson, A. *Science* **2004**, *304*, 995–999.
(7) Korobov, M.; Avramenko, N.; Bogachev, A.; Rozhkova, N.; Ōsawa, E. *J. Phys. Chem. C* **2007**, *111*, 7330–7334.
(8) Febles, M.; Pérez-Hernández, N.; Pérez, C.; Rodríguez, M. L.; Foces-Foces, C.; Roux, M. V.; Morales, E. Q.; Buntkowsky, G.; Limbach, H.-H.; Martín, J. D. *J. Am. Chem. Soc.* **2006**, *128*, 10008–10009.
(9) Vaitheeswaran, S.; Yin, H.; Rasaiah, J.; Hummer, G. *Proc. Natl. Acad. Sci. U.S.A.* **2004**, *101*, 17002–17005.
(10) Sun, T.; Feng, L.; Gao, X.; Jiang, L. *Acc. Chem. Res.* **2005**, *38*, 644–652.
(11) Mashl, R. J.; Joseph, S.; Aluru, N. R.; Jakobsson, E. *Nano Lett.* **2003**, *3*, 589–592.
(12) Naguib, N.; Ye, H.; Gogotsi, Y.; Yazicioglu, A. G.; Megaridis, C. M.; Yoshimura, M. *Nano Lett.* **2004**, *4*, 2237–2243.
(13) Maniwa, Y.; Kataura, H.; Abe, M.; Udaka, A.; Suzuki, S.; Achiba, Y.; Kira, H.; Matsuda, K.; Kadowaki, H.; Okabe, Y. *Chem. Phys. Lett.* **2005**, *401*, 534–538.
(14) Tan, H. S.; Piletic, I. R.; Riter, R. E.; Levinger, N. E.; Fayer, M. D. *Phys. Rev. Lett.* **2005**, *94*, 057405.
(15) de Groot, B. L.; Grubmuller, H. *Science* **2001**, *294*, 2353–2357.
(16) Tajkorshid, E.; Nollert, P.; Jensen, M. O.; Miercke, L. J.; O'Connell, J.; Stroud, R. M.; Schulten, K. *Science* **2002**, *296*, 525–530.
(17) Zhu, F.; Tajkorshid, E.; Schulten, K. *Biophys. J.* **2004**, *86*, 50–57.
(18) Vidossich, P.; Cascella, M.; Carloni, P. *Proteins* **2004**, *55*, 924–931.
(19) Hummer, G.; Rasaiah, J. C.; Noworyta, J. P. *Nature* **2001**, *414*, 188–190.
(20) Beckstein, O.; Biggins, P. C.; Sansom, M. S. P. *J. Phys. Chem. B* **2001**, *105*, 12902–12905.
(21) Berezhkovskii, A.; Hummer, G. *Phys. Rev. Lett.* **2002**, *89*, 064503–1.
(22) Waghe, A.; Rasaiah, J. C.; Hummer, G. *J. Chem. Phys.* **2002**, *117*, 10789–10795.
(23) Koga, K.; Gao, G. T.; Tanaka, H.; Zeng, X. C. *Physica A* **2002**, *314*, 462–469.
(24) Noon, W. H.; Ausman, K. D.; Smalley, R. E.; Ma, J. *Chem. Phys. Lett.* **2004**, *355*, 445–448.
(25) Allen, R.; Melchionna, S.; Hansen, J. P. *Phys. Rev. Lett.* **2002**, *89*, 175502–1.
(26) Allen, R.; Hansen, J. P.; Melchionna, S. *J. Chem. Phys.* **2003**, *119*, 3905–3919.
(27) Allen, R.; Melchionna, S.; Hansen, J. P. *J. Phys.: Condens. Matter* **2003**, *15*, S297–S302.
(28) Kalra, A.; Garde, S.; Hummer, G. *Proc. Natl. Acad. Sci. U.S.A.* **2003**, *100*, 10175–10180.
(29) Beckstein, O.; Sansom, M. S. P. *Proc. Natl. Acad. Sci. U.S.A.* **2003**, *100*, 7063–7068.
(30) Zhu, F.; Schulten, K. *Biophys. J.* **2003**, *85*, 236–244.
(31) Vaitheeswaran, S.; Rasaiah, J. C.; Hummer, G. *J. Chem. Phys.* **2004**, *121*, 7955–7965.
(32) Wang, J.; Zhu, Y.; Zhou, J.; Lu, X. H. *Phys. Chem. Chem. Phys.* **2004**, *6*, 829–835.
(33) Liu, Y.; Wang, Q.; Lu, L. *Langmuir* **2004**, *20*, 6921–6926.
(34) Beckstein, O.; Sansom, M. S. P. *Phys. Biol.* **2004**, *1*, 42–52.
(35) Kolesnikov, A. I.; Zanotti, J. M.; Loong, C. K.; Thiyagrarajan, P.; Moravsky, A. P.; Loutfy, R. O.; Burnham, C. J. *Phys. Rev. Lett.* **2004**, *93*, 035503–1.
(36) Huang, B.; Xia, Y.; Zhao, M.; Li, F.; Liu, X.; Ji, Y.; Song, C. *J. Chem. Phys.* **2005**, *122*, 084708.
(37) Giovambattista, N.; Debenedetti, P. G.; Rossky, P. J. *J. Phys. Chem. C* **2007**, *111*, 1323–1332.
(38) Whitby, M.; Quirke, N. *Nat. Nanotechnol.* **2007**, *2*, 87–94.

(39) Joseph, S.; Mashl, R. J.; Jakobsson, E.; Aluru, N. R. *Nano Lett.* **2003**, *3*, 1399–1403.
(40) Qiao, R.; Aluru, N. *Colloids Surf. A* **2005**, *267*, 103–109.
(41) Raghunathan, A.; Aluru, N. R. *Phys. Rev. Lett.* **2006**, *97*, 024501.
(42) Dzubiella, J.; Allen, R.; Hansen, J. P. *J. Chem. Phys.* **2004**, *120*, 5001–5004.
(43) Yang, L.; Garde, S. *J. Chem. Phys.* **2007**, *126*, 084706.
(44) Piletic, I.; Moilanen, D.; Spry, D.; Levinger, N.; Fayer, M. *J. Chem. Phys. A* **2006**, *110*, 4985–4999.
(45) Cringus, D.; Bakulin, A.; Linder, J.; Vöhringer, P.; Pshenichnikov, M.; Wiersma, D. *J. Phys. Chem. B* **2007**, *111*, 14193–14207.
(46) Chanda, J.; Bandyopadhyay, S. *J. Phys. Chem. B* **2006**, *110*, 23443–23449.
(47) Allen, M. P.; Tildesley, D. J. *Computer Simulation of Liquids*; Clarendon Press: Oxford, U.K., 1987.
(48) Phillips, J.; Braun, R.; Wang, W.; Gumbart, J.; Tajkhorshid, E.; Villa, E.; Chipot, C.; Skeel, R.; Kale, L.; Schulten, K. *J. Comput. Chem.* **2005**, *26*, 1781–1802.
(49) Humphrey, W.; Dalke, A.; Schulten, K. *J. Mol. Graph. Model.* **1996**, *14*, 33–38.
(50) Luzar, A.; Chandler, D. *Phys. Rev. Lett.* **1996**, *76*, 928–931.
(51) Starr, F. W; Nielsen, J. K.; Stanley, H. E. *Phys. Rev. E* **2000**, *62*, 579.
(52) Matsumoto, M. *J. Chem. Phys.* **2007**, *126*, 054503.
(53) van der Spoel, D.; van Maaren, P.; Larsson, P.; Tîmneanu, N. *J. Phys. Chem. B* **2006**, *110*, 4393–4398.
(54) Gardillo, M.; Marti, J. *Chem. Phys. Lett.* **2000**, *329*, 341–345.
(55) Kumar, R.; Schmidt, J.; Skinner, J. *J. Chem. Phys.* **2007**, *126*, 204107.
(56) Luzar, A. *Chem. Phys.* **2000**, *258*, 267–276.
(57) Malenkov, G. *J. Struct. Chem.* **2006**, *47*, s5–s31.
(58) Lyubartsev, A.; Laaksonen, A. *J. Phys. Chem.* **1996**, *100*, 16410.
(59) Jinesh, K. B.; Frenken, J. M. W. *Phys. Rev. Lett.* **2008**, *101*, 036101.
(60) Goldsmith, J.; Martens, C. C. *Phys. Chem. Chem. Phys.* Submitted.

JP808709V